Mannosylated solid lipid nanoparticles for the selective delivery of rifampicin to macrophages

Alexandre C. C. Vieira, Luíse L. Chaves, Marina Pinheiro, Sofia A. Costa Lima, Domingos Ferreira, Bruno Sarmento & Salette Reis

Published online: 12 Feb 2018.

Submit your article to this journal ⬚

View related articles ⬚

View Crossmark data ⬚

Taylor & Francis
Taylor & Francis Group

Check for updates

Mannosylated solid lipid nanoparticles for the selective delivery of rifampicin to macrophages

Alexandre C. C. Vieira[a] (iD), Luíse L. Chaves[a] (iD), Marina Pinheiro[a] (iD), Sofia A. Costa Lima[a] (iD), Domingos Ferreira[b] (iD), Bruno Sarmento[c,d,e] (iD) and Salette Reis[a] (iD)

[a]UCIBIO, REQUIMTE, Departamento de Ciências Químicas, Faculdade de Farmácia, Universidade do Porto, Porto, Portugal; [b]UCIBIO, REQUIMTE, Laboratório de Tecnologia Farmacêutica, Departamento de Ciências do Medicamento, Faculdade de Farmácia, Universidade do Porto, Porto, Portugal; [c]I3S, Instituto de Investigação e Inovação em Saúde, Universidade do Porto, Porto, Portugal; [d]INEB – Instituto de Engenharia Biomédica, Universidade do Porto, Porto, Portugal; [e]CESPU, Instituto de Investigação e Formação Avançada em Ciências e Tecnologias da Saúde, Instituto Universitário de Ciências da Saúde, Gandra, Portugal

ABSTRACT

Tuberculosis (TB) is still a devastating disease and more people have died of TB than any other infectious diseases throughout the history. The current therapy consists of a multidrug combination in a long-term treatment, being associated with the appearance of several adverse effects. Thus, solid lipid nanoparticles (SLNs) were developed using mannose as a lectin receptor ligand conjugate for macrophage targeting and to increase the therapeutic index of rifampicin (RIF). The developed SLNs were studied in terms of diameter, polydispersity index, zeta potential, encapsulation efficiency (EE) and loading capacity (LC). Morphology, *in vitro* drug release and differential scanning calorimetry studies, macrophage uptake studies, cell viability and storage stability studies were also performed. The diameter of the SLNs obtained was within the range of 160–250 nm and drug EE was above 75%. The biocompatibility of M-SLNs was verified and the internalization in macrophages was improved with the mannosylation. The overall results suggested that the developed mannosylated formulations are safe and a promising tool for TB therapy targeted for macrophages.

Introduction

Tuberculosis (TB) is an infectious disease caused by the bacillus *Mycobacterium tuberculosis* (MTB) and more people have died of TB than any other infectious disease throughout history [1] . In 2016, World Health Organization (WHO) reported an estimated 10.4 million new cases and 1.8 million deaths from TB, including 0.4 million HIV-positive individuals [2]. TB is caused by the bacillus *Mycobacterium tuberculosis* (MTb), through the inhalation of aerosols and bacilli colonization inside the alveolar macrophages (AMs) [3,4].

Rifampicin (RIF) was introduced in conventional anti-TB regimen in the mid 1960s in combination with other drugs, namely isoniazid, pyrazinamide and ethambutol [5]. However, the long treatment schedules that are required (at least six months) for conventional anti-TB chemotherapy are commonly associated with severe adverse effects, resulting in poor compliance to therapy, which is one of the main reasons for the appearance of multidrug resistant strains and treatment's inefficacy [6–8]. According to this, more effective technologies are required and improving drug delivery strategies for the existing drugs may be determinant to shorten TB treatment duration, avoiding resistance and improving patient compliance to therapy [5]. In this context, emerging technologies in drug delivery, including nanoparticles (NPs) can increase the therapeutic index of drugs [9]. In the TB field

exploiting the NPs as drug delivery systems, the most striking results are related with the reduction of the duration of treatment in animal models. Nonetheless, these NPs have several drawbacks and thereby none of them reach the market. Among other problems, main weaknesses of these delivery systems are the low drug loading capacity (LC), design of the particles independent of the goal (e.g. route of administration and the type of TB pulmonary or extrapulmonary), absence of biocompatibility studies and difficulties to scale-up. In this context, lipid NPs were developed to overcome the disadvantages [5]. In comparison with the above-mentioned NPs, lipid NPs generally show higher LC, higher stability and do not require the use of organic solvents during production and are less expensive to produce [5,10]. In this work, solid lipid nanoparticles (SLNs) were developed to load RIF since they have LC, high stability, do not require the use of organic solvents during production and are relatively inexpensive to produce [5,10]. Further, SLNs were functionalized with mannose [11] to increase the selectivity of the NPs to the AMs, since lectin receptors are highly expressed in the main cell in the macrophages, where MTB is mainly located [12]. Moreover, SLNs were developed to be administered by inhalatory route, which has particular interest in the controlled release of anti-TB drugs directly in the main organ affected by TB (lungs), thus achieving high local concentrations of the drug in the infected macrophages. The developed SLNs were

---

characterized according to their average diameter, polydispersity index, zeta potential, surface morphology, encapsulation efficiency (EE), LC, drug *in vitro* release under different pH conditions, macrophage uptake studies, cell viability and storage studies. The results support that the SLNs developed are promising to improve the TB conventional treatment.

Materials and methods

Materials

RIF (more than 98% pure), stearylamine (97% pure) and D-(+)-Mannose (more than 99% pure) were purchased from Sigma-Aldrich (St Louis, MO, USA). Aerosil® 200 was supplied by Acofarma® (Terrassa, Espanha, Spain.) The SLNs were prepared with glycerol tripalmitate provided by Alfa Aesar (Karlsruhe, Germany), Tween® 80 purchased from Sigma-Aldrich Co. (St Louis, MO, USA). Phorbol 12-myristate 13-acetate (PMA), trypan blue, thiazolyl blue tetrazolium bromide (MTT), phosphate buffered saline pH 7.4 (PBS), sucrose, chlorpromazine hydrochloride, filipin, cytochalasin D and coumarin 6 were obtained from Sigma–Aldrich (St. Louis, MO, USA). All other chemicals used in the study were of analytical grade. Dulbecco's Modified Eagle's Medium (DMEM), Fetal Bovine Serum (FBS) and penicillin-streptomycin antibiotics mixture were purchased from Gibco® (Invitrogen Corporation, London, UK). Human leukemia monocyte THP1 cell line from European Culture Collections (Salisbury, UK).

Preparation of the formulations

Preparation of SLNs

RIF-loaded SLNs and placebo SLNs were prepared by hot ultrasonication method as previously described [13]. Briefly, the lipid phase containing the lipid glycerol tripalmitate and RIF was heated to 75 °C until complete drug solubilization in the lipid matrix. The aqueous phase containing the surfactant (Tween® 80) in double deionized water was previously heated in water bath to the same temperature. The aqueous phase (6 ml) was poured into the lipid phase and homogenized using a probe-sonicator (VCX130, Sonics and Materials, 115 Newtown, CT, USA) in 1 min with 70% of the amplitude. The nanosuspension obtained was rapidly cooled in ice bath with agitation (30 s). Placebo SLNs were prepared in a similar way without the drug.

Preparation of mannosylated SLNs

Mannosylated SLNs (M-SLNs) were obtained according to the section "Preparation of SLNs"2.1 with some modifications. Steryl amine (SA) was added in the lipid phase in the ratio of 2% (w/w) of the lipid, and all the subsequent steps were exactly as described before to obtain a modified SLNs (M-SLNs). The mannose coating was carried out according to the previous methods [11,14,15]. Briefly, a known volume of a solution of D-mannose (50 mM) in acetate buffer (pH 4) was added to the SLNs, and the mixture was maintained in agitation with magnetic stirring at room temperature for 48 h to achieve maximum conjugation. M-SLNs were subjected to dialysis bag (dialysis bag; MWCO 12–14 kDa) in high volume of double distilled water for 30 min to remove unreacted mannose or other impurities.

Lyophilization

The obtained placebo and RIF-loaded SLNs and M-SLNs were freeze dried using Aerosil® as cryoprotectant, at the amount of 2% (w/w) to the lipid to minimize the freeze-drying process and protect the NPs from the mechanical stress of ice crystals [15,16]. The lyophilization protocol was adapted from the method described by Pinheiro et al. [11]. All nanosuspensions were poured into semi-stoppered glass vials with slotted rubber closures and frozen at -80 °C (Deep freezer, GFL®, Hannover, Germany) and then were transferred to lyophilization (LyoQuest −85 plus v0.407, Telstar, Terrassa, Spain) for 48 h at −80 °C under 0.40 mbar of pressure. After lyophilization, all samples were stored in controlled environment of temperature and humidity.

Characterization of the formulations

Particles' diameter and polydispersity index

The hydrodynamic diameter and the width of distribution (polydispersity index, PDI) of placebo and RIF-loaded SLNs and M-SLNs were analyzed using a dynamic light scattering (DLS) (Brookhaven Instruments, Holtsville, NY, USA), operating at a scattering angle of 90°. All samples were diluted (1:200) with double distilled water to reach a suitable concentration before measurement (kcps 300–500).

Zeta potential

The zeta potential of placebo and RIF-loaded SLNs and M-SLNs was measured by an electrophoretic analyser from Zeta Potential Analyzer (Brookhaven Instruments, Holtsville, NY, US). All samples were diluted with double distilled water, the electrode was coupled in cuvettes, which were applied to an electric field to analyse the surface charge. All measurements were performed at room temperature.

Encapsulation efficiency and loading capacity

The EE and LC of RIF within SLNs and M-SLNs was determined by the indirectly method as previously described [11,15]. Briefly, a known aliquot of NPs were properly diluted and submitted to centrifugation with Amicon® (Merck KGaA, Darmstadt, Germany) filter device. The non-encapsulated drug was quantified by UV spectroscopy at 334 nm [17]. A standard curve was used to determine the concentration of RIF and the results are expressed as mean ± standard deviation ($n = 3$).

$$EE = \frac{Initial\ RIF - Recovered\ RIF}{Initial\ RIF} \times 100$$

$$LC = \frac{Initial\ RIF - Recovered\ RIF}{Total\ amount\ of\ lipid} \times 100$$

Transmission electron microscopy (TEM)

The morphology of placebo and RIF-loaded SLNs and M-SLNs was observed by TEM (TEM Jeol JEM-1400; JEOL Ltd., Tokyo, Japan). Images were obtained after one drop of fresh NPs over a grid followed by negative staining with uranyl acetate and subjecting it to an accelerating voltage of 60 kV.

Fourier transform infrared spectroscopy (FTIR)

The freeze-dried optimized placebo and RIF-loaded SLNs and M-SLNs, and pure RIF were evaluated using an FTIR Spectrophotometer (Frontier TM, PerkinElmer; Santa Clara, CA, USA) equipped with a horizontal attenuated total reflectance (ATR) sampling accessory with a diamond crystal. The samples were transferred directly to the ATR compartment, and the result was obtained by combining the 32 scans. The spectra were recorded between 4000 and 600 cm^{-1} with a resolution of 2 cm^{-1}.

Differential scanning calorimetry (DSC)

DSC measurements were performed using DSC 200 F3 Maia®, Netzsch, Hannover (Germany). Approximately 7 mg of binary mixtures or an equivalent amount of RIF were weighed in an aluminum pan and sealed. For the placebo and RIF-loaded SLNs and M-SLNs, known amounts of the selected formulations were weighed and similarly sealed in aluminum pans. The reference pan was left empty. Heating curves for the drug and the mixtures of drug and lipid were recorded with a heating rate of 10 °C/min from 15 °C to 300 °C and then cooled to 25 °C, under liquid nitrogen, with cooling rate of 40 °C/min. The onset, melting point (peak maximum) and enthalpy (ΔH) were calculated using the software provided by the DSC equipment.

In vitro release study

The release profiles of RIF-loaded SLNs and M-SLNs were investigated by simulating the release of drug under pulmonary environment [18]. For this purpose, buffered solutions at three different pH values (4.5, 6.2 and 7.4) were used to simulate the phagosome, phagolysosome and the *in vitro* physiological conditions, respectively [11].

In vitro release studies were performed using the dialysis bag method in sink conditions. The NPs were first poured into the dialysis bag (molecular weight cut off 6000–8000 Da, CelluSep; Membrane Filtration Products Inc., Frilabo, Maia, Portugal) with the two ends fixed by thread and placed into the preheated dissolution media. The suspension was stirred at 37 °C, using a heating and magnetic stirring plate (IKAMAG1, Staufen, Germany) at 350 rpm. At fixed time intervals, 200 μL of sample was withdrawn and the same volume of fresh buffer was added accordingly to the condition. The samples were read in a UV 96-well plate reader (Synergy™ HT, Biotek, Winooski, USA), at 334 nm. All the analytical conditions were previously optimized, and standard curves were obtained in triplicate.

The RIF release profiles were evaluated in each pH condition and the profiles were compared using the kinetics models of the release profile by fitting in different equations such as zero order, first order, Higuchi, Korsemeyer–Peppas and Hixson–Crowell. The determination of the kinetic models aimed to give a preliminary indication of the drug localization inside the lipid matrix and the degree of organization of the NPs for both SLNs-RIF and M-SLNs-RIF [19,20].

Storage stability

To evaluate the stability of optimized SLNs-RIF and M-SLNs-RIF NPs, a study was carried out regarding particle diameter, PDI and zeta potential for a period of six months. The NPs were stored at room temperature and compared to the first day of production, as described earlier.

Cellular studies

In vitro cytotoxicity

Human THP1 monocytes were seeded at a density of 10^5 cells/well and grown in DMEM supplemented with fetal bovine serum and penicillin/streptomycin at 37 °C with 5% CO_2. THP1 monocytes were differentiated into macrophages after 18 h with 20 ngmL^{-1} phorbol 12-myristate 13-acetate (PMA), followed by 24 h with fresh supplemented culture medium.

The THP1 differentiated macrophages viability was assessed upon treatment with SLNs and M-SLNs unloaded and RIF-loaded, and pure RIF using a MTT (thiazolyl blue tetrazolium blue) assay. After 24 h of incubation, the medium was replaced by MTT (0.5 mg mL^{-1} in culture medium) for 3 h at 37 °C. Then, the medium was removed and equal volume of DMSO was added to dissolve the formed formazan crystals. The optical density of the supernatant was read at 570 nm and 630 nm using a microplate spectrophotometer (Synergy™ HT, Biotek, USA). Results were expressed as the percentage of the metabolic activity of treated cells relative to untreated cells.

Cellular uptake studies and intracellular pathways

For the cellular internalization assay, the SLNs and M-SLNs were labelled with coumarin 6 (C6) by the addition of this molecule to the lipid phase during the preparation process, as described in 2.2. The resulting SLNs-C6 and M-SLNs-C6 exhibited identical size and surface potential as SLNs and M-SLNs loaded with RIF. The cellular uptake of NPs-C6 was evaluated in THP1 differentiated macrophages upon incubation with SLNs and M-SLNs (100 μg mL^{-1}). After specific times, cells were washed with PBS to remove non-internalized NPs, recovered in 0.2 ml of PBS containing with 0.11% Trypan blue and incubated for 1 min in order to quench the C6-fluorescent signal coming from SLNs adsorbed to the cell surface. Cells were examined under the 488 nm excitation and 520 nm emission wavelengths in the flow cytometer (Accuri™ C6, BD Biosciences, Erembodegem, Belgium). Dead cells were excluded with propidium iodide staining. For each sample, a minimum of 10,000 events were recorded and the auto-fluorescence of non-treated cells were used as control. The uptake data were curve-fitted to the Michaelis − Menten equation using GraphPad Prism 7 (La Jolla, CA, USA), and the Michaelis

constant rate (K) as well as the maximal uptake rate (V_{max}) were determined.

The internalization pathways involved in the cellular uptake of SLNs and M-SLNs was also studied in human macrophages using flow cytometry. Briefly, upon THP1 differentiation in macrophages, the cells were pre-incubated for 30 min at 37°C with 5% CO_2 with three pharmacological pathway inhibitor solutions: chlorpromazine ($10 \mu gmL^{-1}$), filipin ($1 \mu gmL^{-1}$) or cytochalasin D ($5 \mu gmL^{-1}$) [21]. After 1 h incubation with SLNs-C6 or mSLNs-C6, with or without treatment, the cells were recovered in fresh DMEM as previously described. The results were reported as mean fluorescence intensity (MFI) of cells with inhibitor and normalized relatively to the auto-fluorescence of cells incubated with no inhibitor at 37°C used as control.

Statistical analysis

Statistical analyses were performed using IBM® SPSS® Statistics software (v.22.0.0.0; IBM, Armonk, NY, USA). The measurements were repeated at least three times and data expressed as mean ± SD. Data were analyzed using one-way analysis of variance (ANOVA) and the differences between groups compared by Bonferroni, Tukey and Dunnet *post-hoc* tests with GraphPad Prism 6 software (La Jolla, CA, USA). The differences were considered to be significant when the *p* values was < .05.

Results and discussion

Characterization of the formulations

The main physicochemical characteristics of the SLNs developed in this study are listed in Table 1. All SLNs except M-SLNs-RIF were relatively small in size, in the range of 160–168 nm, suggesting that drug incorporation and mannosylation process themselves did not influence the formulations size. Contrastingly, both processes in combination induced a significant increment of the particles diameter ($p < .05$), i.e. M-SLNs-RIF presented a diameter of 252 ± 2 nm, which was larger than SLNs-RIF (160 ± 9 nm) and M-SLNs (168 ± 2 nm). Moreover, the obtained particles' diameter was suitable for pulmonary administration and for macrophages internalization [22,23]. The suspension of all developed NPs was monodisperse with a PDI below 0.2 (Table 1), indicating the homogeneous distribution of the SLNs [24].

The zeta potential values obtained for SLNs and SLNs-RIF were close to -30 mV. Thus, the incorporation of the drug did not considerably affect the surface charge of the SLNs.

On the other hand, the presence of mannose leads to formulation with positive surface charge ($+38.0 \pm 1.1$ mV and $+25.7 \pm 3.5$ mV for M-SLNs and M-SLNs-RIF, respectively). This change of surface potential from negative to positive charge supports the process of mannosylation since it involves the addition of stearylamine to have amine groups on the surface of the NPs [15]. In addition, the developed SLNs possess a high absolute zeta potential and for that reason, they are considered physically stable due to the electrostatic repulsions between NPs [25].

The EE of drug in SLNs was found to be considerably high (above 70%). The mannosylation process induced a significant increase in the EE values ($p < .05$) and the EE obtained for these NPs was higher than 90%. The LC of RIF obtained for SLNs and M-SLNs was 2.7 ± 0.2 and 3.5 ± 0.6%, respectively. The high EE and LC values indicate that the lipid composition of the NPs is appropriate for RIF incorporation and delivery.

Functionalization of SLNs with mannose

Figure 1 shows the spectra of RIF, SLNs, M-SLNs and the correspondent physical mixture (PM). SLNs and RIF-SLNs do not display any band characteristic of mannose functionalization (Figure 2(A)), presented only in the M-SLNs and M-SLNs-RIF (Figure 2(B,C)). The process of functionalization was made by the opening of the mannose ring and following reaction of its aldehyde group with free amine functionalities present over the surface of SLNs. This leads to the formation of Schiff's base (–N=CH–), detectable by FTIR spectroscopy at the wavelength of $\sim 1567 cm^{-1}$, as can be observed in Figure 2(B), and in more detail, in Figure 2(C). Similar results were obtained in the previous studies [14].

Transmission electron microscopy

Transmission electron microscopy (TEM) studies were performed to evaluate the morphological characteristics of all SLNs. TEM imaging revealed spherical NPs (Figure 2). Despite the spherical shape of all SLNs, it can be observed from Figure 2 that both SLNs-RIF (Figure 2(B)), M-SLNs (Figure 2(C)), and M-SLNs-RIF (Figure 2(D)) exhibit a more irregular spherical shape than SLNs (Figure 2(A)), indicating that the incorporation of the RIF and/or the mannosylation process induce slight alterations in the SLNs' morphology. The images demonstrated that all SLNs presented a narrow diameter distribution with particle diameter near 200 nm.

In vitro *release study*

The *in vitro* release of RIF from SLNs and M-SLNs was measured in phosphate buffer at different pH conditions to simulate the passage of the NPs following pulmonary administration. The study was conducted in simulated lung fluid (phosphate buffer, pH 7.4), physiological pH of the nasal fluid and phagosomes (phosphate buffer, pH 6.2) and, also the acidic vesicles phagolysosomes (pH 4.5) where the bacteria is located inside the macrophages [11]. From the analysis of Figure 3, it is possible to observe a slow drug release
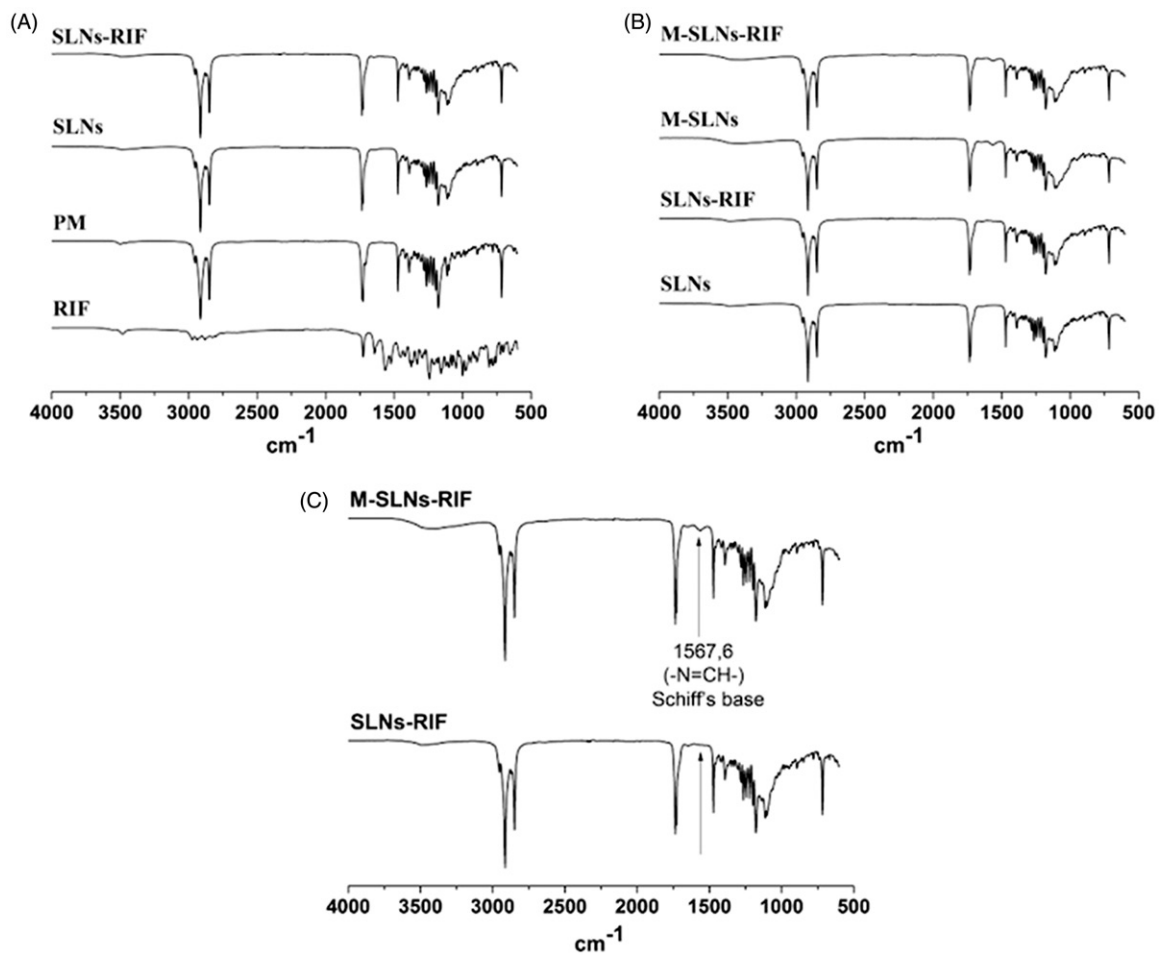
Table 1. Mean hydrodynamic particle size, polydispersion index (PDI), zeta potential, EE and LC of SLNs, SLNs-RIF, M-SLNs and M-SLNs-RIF.

Samples	Diameter (nm)	PDI	ZP (mV)	EE (%)	LC (%)
SLNs	163 (±9)	0.17 (±0.02)	−31.3 (±0.9)	N.A.	N.A.
SLNs-RIF	160 (±9)	0.12 (±0.03)	−25.4 (±0.8)	74.0 (±5.9)	2.7 (±0.2)
M-SLNs	168 (±2)	0.16 (±0.01)	+38.0 (±1.1)	N.A.	N.A.
M-SLNs-RIF	252 (±2)	0.17 (±0.01)	+25.7 (±3.5)	95.5 (±6.0)	3.5 (±0.6)

M-SLN-RIF: rifampicin-loaded mannosylated solid lipid nanoparticles; M-SLNs: mannosylated solid lipid nanoparticles; SLN RIF: rifampicin-loaded solid lipid nanoparticles; SLNs: solid lipid nanoparticles; RIF: rifampicin.

Figure 1. Infrared spectra of RIF, PM, SLNs, SLNs-RIF, M-SLNs and M-SLNs-RIF ($n = 3$). (A) RIF, PM, SLNs and SLNs-RIF. (B) SLNs, SLNs-RIF, M-SLNs and M-SLNs-RIF. (C) M-SLNs-RIF and SLNs-RIF and Schiffs base. M-SLN-RIF: rifampicin-loaded mannosylated solid lipid nanoparticles; M-SLNs: mannosylated solid lipid nanoparticles; SLN RIF: rifampicin-loaded solid lipid nanoparticles; SLNs: solid lipid nanoparticles; PM: physical mixture; RIF: rifampicin.
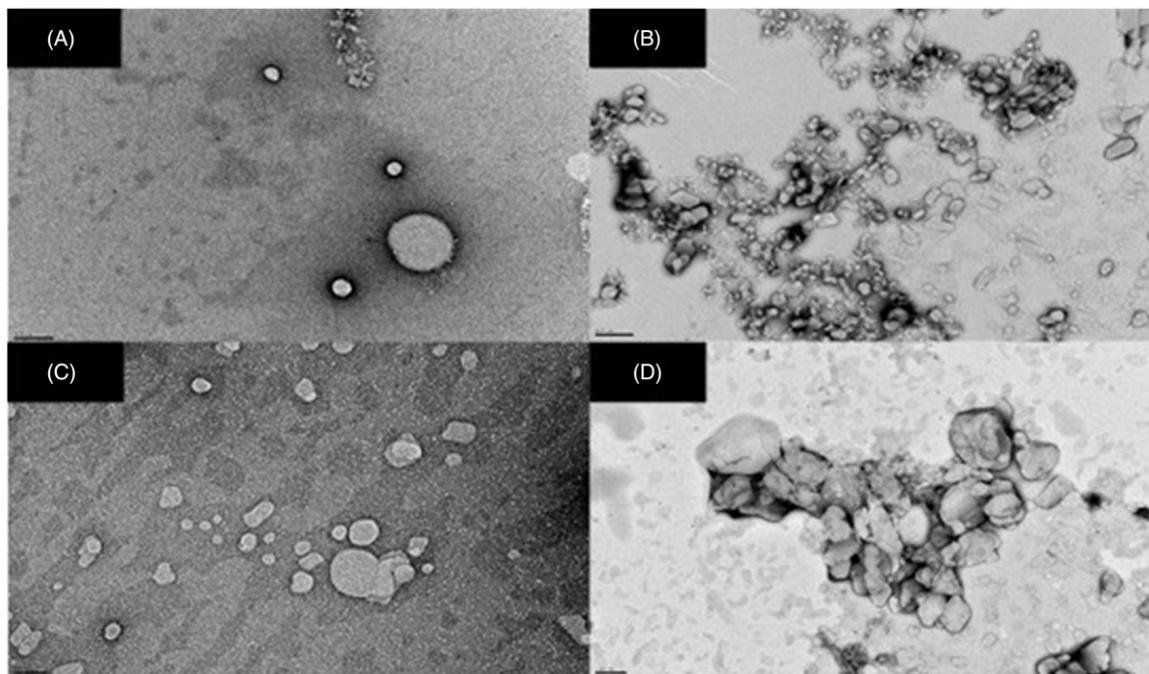

Figure 2. Transmission electron photomicrographs of (A) SLNs, (B) SLN-RIF, (C) M-SLNs and (D) M-SLN-RIF ($n = 3$). (Scale bar: 200 nm). M-SLN-RIF: rifampicin-loaded mannosylated solid lipid nanoparticles; M-SLNs: mannosylated solid lipid nanoparticles; SLN RIF: rifampicin-loaded solid lipid nanoparticles; SLNs: solid lipid nanoparticles.
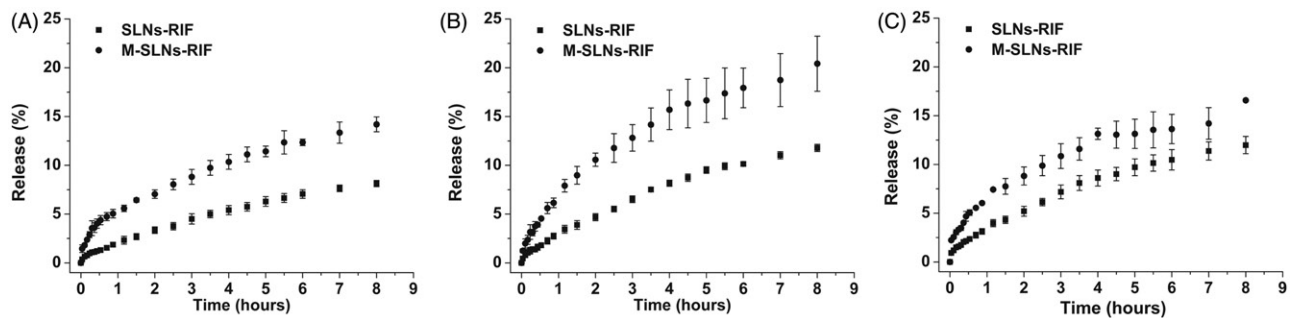
Figure 3. *In vitro* RIF release profile of SLNs-RIF and M-SLN-RIF in pH 7,4 (A), pH 6,2 (B) and pH 4,5 (C), in order to simulate the release of the drug in following pulmonary administration until it has reached the acidic vesicles phagosomes and phagolysosomes ($n = 3$). RIF: rifampicin; M-SLNs-RIF: rifampicin-loaded mannosylated solid lipid nanoparticles; SLNs-RIF: rifampicin-loaded solid lipid nanoparticles.
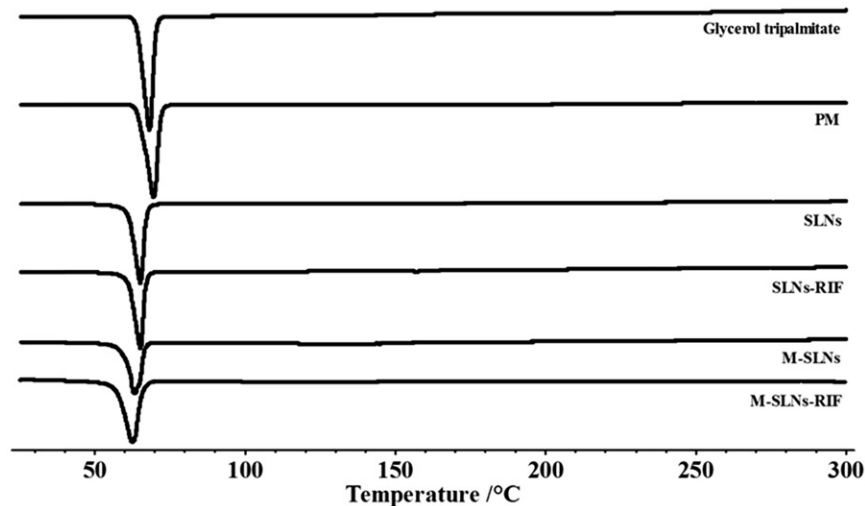

Figure 4. DSC thermograms Infrared spectra of Glycerol palmitate, PM, SLNs, SLNs-RIF, M-SLNs and M-SLNs-RIF ($n = 3$). M-SLN-RIF: rifampicin-loaded mannosylated solid lipid nanoparticles; M-SLNs: mannosylated solid lipid nanoparticles; SLN RIF: rifampicin-loaded solid lipid nanoparticles; SLNs: solid lipid nanoparticles; PM: physical mixture.

profile from SLNs, being only 10% of drug released from the SLNs within the first 4 h. The drug release increases slowly during time, being below 20% at 8 h. From Figure 3, it can be observed that the drug release in both SLNs-RIF and M-SLNs-RIF is pH-dependent with a faster drug release at acidic pH than at physiological pH. These results point that the majority of the drug (80% or more) remained entrapped in SLNs and M-SLNs after their contact with the pulmonary mimetic conditions, and able to be released inside the infected cells, which reinforces that both SLNs and specially functionalized SLNs are suitable NPs for the pulmonary delivery of RIF, protection from the degradation and ultimately enhancing drug bioavailability.

The difference between SLNs-RIF and M-SLNs-RIF release profiles suggest that the nanocarriers have distinct structures. The mannose coating of the M-SLNs-RIF contributed to increase the disorder of the SLNs structure, creating a more irregular matrix, corroborating with DSC analysis (Figure 4), leading to a faster release of RIF in M-SLNs-RIF (Figure 3).

The release profiles of SLNs-RIF and M-SLNs in different pH (7.4, 6.2 and 4.5) were studied by analyzing the regression coefficients (R^2) obtained after fitting into zero order, first order, Hixson–Crowell, Higuchi and Korsmeyer–Peppas release kinetics models, in Table 2 [26]. Based on the obtained results, the Higuchi model was found to be the best model as it presented higher values of R^2 (0.996, 0.996 and 0.992) for the three pH conditions. This mathematical model proposes a direct relation of the drug release from the matrix to a square root of time [26]. Thus, RIF release from SLNs andM-SLNs occurs by a diffusion-controlled process.

Lipid matrix analysed by DSC

The interactions between lipid NPs and incorporated drugs commonly result in alterations in melting temperatures and melting enthalpies (ΔH) [27]. Moreover, the surface coating has also been reported to alter calorimetric parameters in NPs [28]. Thus, DSC analysis was performed to study the alterations in the lipid matrix of SLNs after the incorporation of RIF and mannose ligand. The DSC thermograms obtained for all SLNs formulations and for the pure solid lipid and physical mixture are depicted in Figure 4, while the respective melting parameters are shown in Table 3.

As expected, the onset temperature and the melting enthalpy (ΔH) of SLNs were lower in comparison to the bulk solid lipid with the physical mixture, which may be explained by the interactions that occur between the solid lipid and

Table 2. Results of the kinetic parameters of the drug release profile obtained for M-SLN-RIF: determination coefficient (R^2).

Release sample I pH		Release model				
		Zero order	First order	Hixson–Crowel	Higuchi	Korsmeyer–Peppas
M-SLNs-RIF	pH 7.4	R2 = 0.944	R2 = 0.765	R2 = 0.649	R2 = 0.996	R2 = 0.944
	pH 6.2	R2 = 0.925	R2 = 0.677	R2 = 0.661	R2 = 0.996	R2 = 0.925
	pH 4.5	R2 = 0.916	R2 = 0.703	R2 = 0.614	R2 = 0.992	R2 = 0.916

M-SLN-RIF: rifampicin-loaded mannosylated solid lipid nanoparticles.

Table 3. Differential scanning calorimetry parameters of SLNs, SLNs-RIF, M-SLNs and M-SLNs-RIF.

Samples	ΔH (J/g)	Melting point (°C)	ΔT_{onset} (°C)	ΔT_{End} (°C)
Glycerol tripalmitate	181.3	68.0	63.9	70.2
PM	172.8	69.4	65.0	71.7
SLNs	125.3	65.0	61.0	67.1
SLNs-RIF	117.0	65.1	61.1	66.9
M-SLNs	105.6	63.2	61.1	66.5
M-SLNs-RIF	70.1	62.4	57.7	35.7

M-SLN-RIF: rifampicin-loaded mannosylated solid lipid nanoparticles; M-SLNs: mannosylated solid lipid nanoparticles; SLN RIF: rifampicin-loaded solid lipid nanoparticles; SLNs: solid lipid nanoparticles; RIF: rifampicin.

surfactant, or increase in surface area of the NPs. The drug loaded and functionalized SLNs showed an onset melting transition peak temperature and a melting enthalpy (ΔH) lower than that of the SLNs, suggesting that RIF and mannose induce disorder in the crystal structure of the NPs. The decrease in the onset temperature and in melting enthalpy (ΔH) was more evident when the two compounds were present together, suggesting a higher disturbance of the SLNs.

Storage stability

The physical stability of all SLNs was verified periodically by analysing the variation of the hydrodynamic diameter, polydispersity, zeta potential and EE during storage conditions for six months at room temperature (Figure 5). For all SLNs, no aggregation was found through visual observations as expected regarding their high zeta potential. According to Figure 5, no tendency to zeta potential variations was observed for the SLNs-RIF and M-SLNs-RIF, supporting the long-term stability of the developed SLNs [15]. In fact, the overall results show that all SLNs are stable for at least six months since only slight variations ($p > .05$) occur in the particles diameter, polydispersity, zeta potential and EE. Thus, the developed SLNs are appropriate for RIF incorporation and for the release prevention during shelf conditions of storage at room temperature.

In vitro cytotoxicity

The cell viability of the placebo and RIF-loaded SLNs and M-SLNs towards THP1 differentiated macrophages was evaluated for 24 h. As shown in Figure 6, treatment with unloaded SLNs up to 0.12 mg mL^{-1} did not affect the cell viability, exhibiting over 80% viability for the studied conditions. Thus, RIF-loaded SLNs and M-SLNs could be used as a delivery system up to this concentration, which corresponds to 57 µg mL^{-1}. In addition, RIF-loaded SLNs and M-SLNs and free RIF solution lead to a similar reduction on the cell viability assessed by a decrease on the mitochondrial metabolism

using the MTT assay (Figure 6). In fact, these results indicate that with the developed SLNs, it is possible to reach a concentration higher than that reported by RIF bactericidal concentration (3.2 µg mL^{-1}) [29]. To proceed with the biological assays, a non-toxic concentration was selected.

Cellular uptake studies and intracellular pathways

Energy may be involved in the process of NPs' cellular internalization. To evaluate the role of energy, THP1 differentiated macrophages were treated with 37 °C, 4 °C and sodium azide, both inhibitors of active transport and then incubated with SLNs and M-SLNs C6-labelled [30]. At lower temperatures (4 °C), the macrophages exhibit a decrease on their cellular fluorescence with either SLNs-C6 (28%) and M-SLNs-C6 (49%), as observed in Figure 7(A). After the sodium azide treatment, the THP1 macrophages incubated with SLNs-C6 did not show a statistical difference ($p > .05$) on the NPs internalization in relation to the control cells (37 °C treatment). The internalization of M-SLNs-C6 by macrophages treated with sodium azide was reduced to 78% ($p < .01$). By lowering the temperature to 4 °C, both cellular active transport and diffusion are compromised, while with sodium azide, only active transport is inhibited. It may be inferred that about 65% of SLNs uptake occurs by passive diffusion, while 30% of M-SLNs are internalized by the same process. Others have described lipid SLNs' uptake dependence on energy with identical outcomes [31–33].

The uptake of SLNs was evaluated using THP1 differentiated macrophages, to unravel the characteristics of this transport system related to intracellular drug delivery. Cellular uptake kinetics was assessed by intracellular fluorescence over an incubation period using flow cytometry. The concentration of SLNs (100 µg mL^{-1}) used does not affect the viability of the cells (Figure 6). As observed in Figure 7(B), NPs' cell entry occurs as early as 15 min, upon incubation at 37 °C, which reveals that SLNs and M-SLNs translocate quickly into the cell, and the time for half-maximal uptake was found to be 1.1 ± 0.2 h. The cellular uptake of SLNs and M-SLNs follows Michaelis–Menten kinetics (Figure 7(B)), and their differences were analyzed by the parameters (Y_{max} and K) on Figure 7(B). M-SLN exhibited a 1.2-fold higher Y_{max} than non-mannosylated SLNs. Concerning the uptake rate constant (K), a smaller value reflects a quicker cellular internalization. In fact, the mannosylation of SLNs resulted in higher uptake by THP1 differentiated macrophages. An analogous behavior was already described for polymeric nanoparticles. Indeed, few studies have also demonstrated the effectiveness of targeting mannose receptors, by conjugating a carbohydrate to polymeric NPs, to activate macrophages towards a robust action against other intracellular pathogens [21,34].
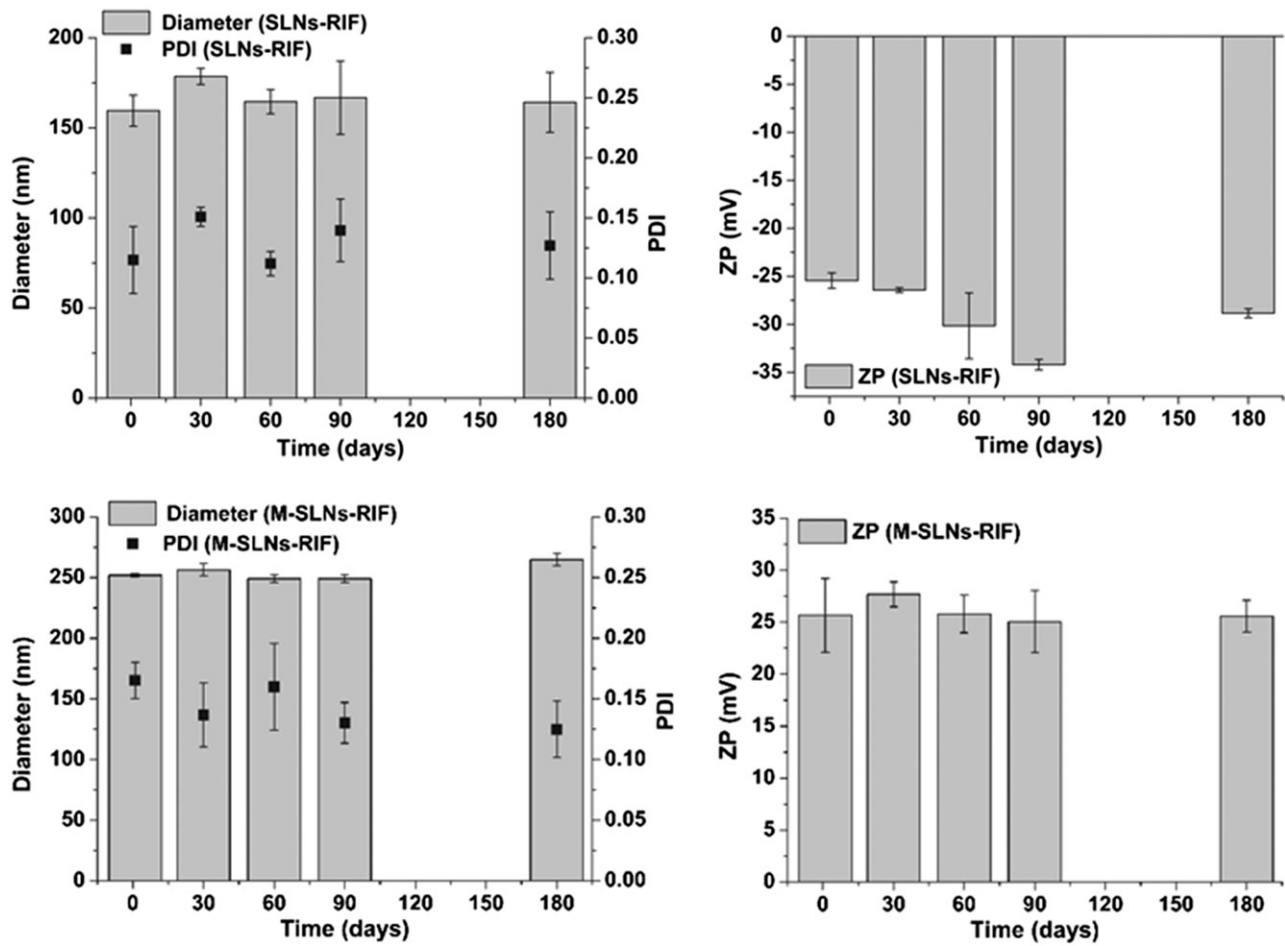
Figure 5. Effect of storage time (at room temperature) on particle diameter, PDI and zeta-potential (ZP) of SLNs-RIF and M-SLNs-RIF during 180 days (mean ± SD, $n = 3$). SLNs-RIF: rifampicin-loaded solid lipid nanoparticles; M-SLNs-RIF: rifampicin-loaded mannosylated solid lipid nanoparticles; PDI: polydispersity index; SD: standard deviation; ZP: zeta potential.
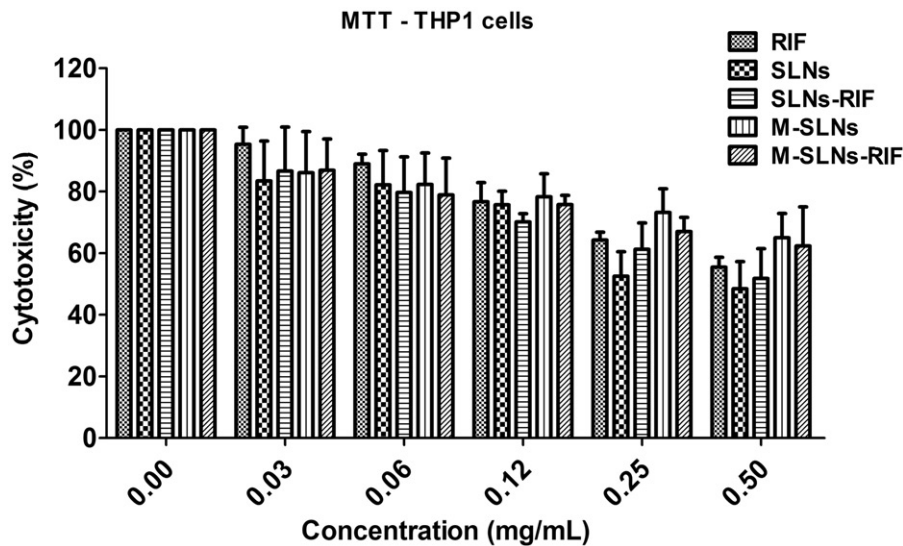

Figure 6. Cell viability of THP1 differentiated macrophages upon exposure to free RIF, placebo and RIF-loaded SLNs and M-SLNs. Data expressed as average ± standard deviation ($n = 5$ of three independent assays). RIF: rifampicin; SLNs: solid lipid nanoparticles; SLNs-RIF: rifampicin-loaded solid lipid nanoparticles; M-SLNs: mannosylated solid lipid nanoparticles; M-SLNs-RIF: rifampicin-loaded mannosylated solid lipid nanoparticles.

To study the endocytic pathways mechanisms involved in the active NPs internalization process, cells were pre-incubated with three pharmacological pathway inhibitors: chlorpromazine and filipin, respectively for clathrin- and caveolae-dependent endocytosis, and cytochalasin D for macropinocytosis [35]. Data exhibited on Figure 7(A) reveal that in THP1 macrophages, the inhibition of clathrin-mediated endocytosis by chlorpromazine led to 40 and 65%
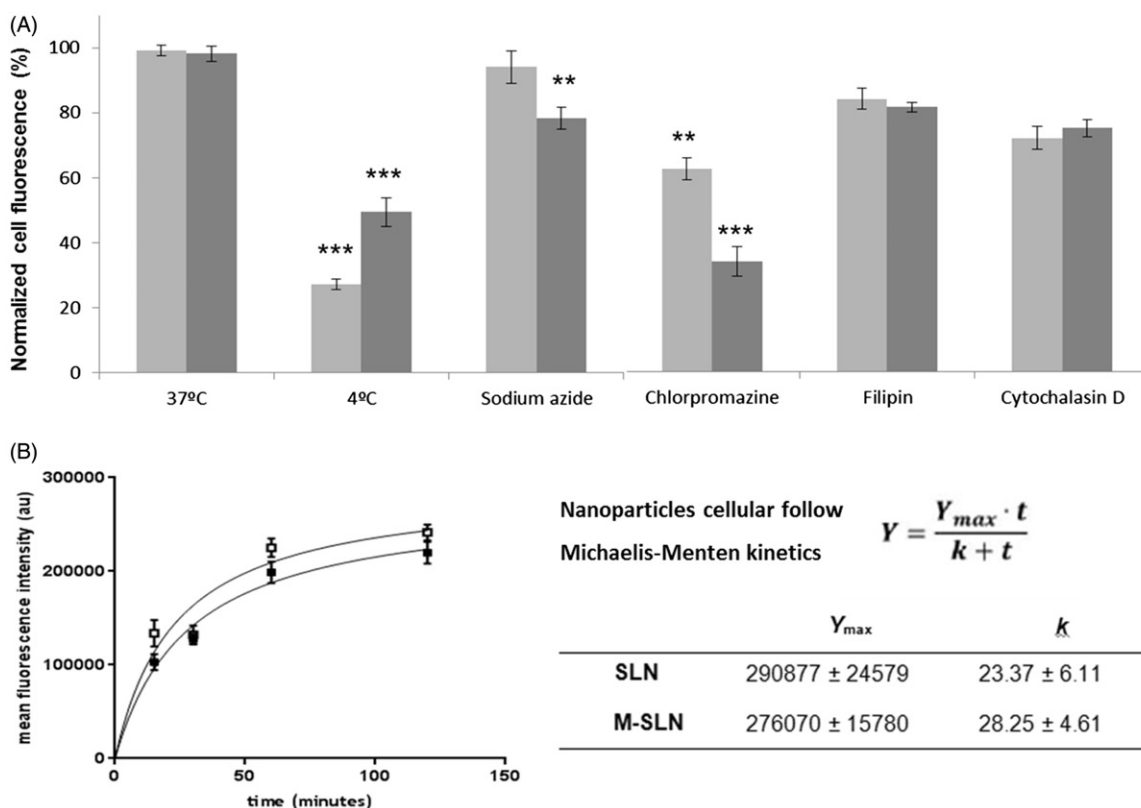
Figure 7. Cellular interaction of nanoparticles on THP1 macrophages. (A) Role of energy in the internalization of SLNs (light grey) and M-SLNs (dark grey), using 37 °C as control. (B) Cellular uptake kinetic profiles obtained by flow cytometry for SLNs (□) and M-SLNs (■). Data expressed as mean ± SD ($n = 3$). Statistical differences in relation to control (37 °C) represented as **$P < .01$ and ***$P < .001$.

reduction on the uptake of SLNs and M-SLNs, respectively. Inhibition of caveolae-mediated endocytosis by filipin resulted in less than 20% inhibition for both lipid NPs studied. Further results revealed that the inhibition of the macropinocytosis process resulted in about 30 and 25% reduction of SLNs and M-SLNs, respectively. Overall, M-SLNs uptake process by human THP1 macrophages in the presence of chlorpromazine exhibited a higher inhibitory effect when compared with the other pathway inhibitory treatments ($p < .01$ for SLNs and $p < .001$ for M-SLNs), thus suggesting a predominant clathrin-mediated endocytic uptake of mannosylated SLNs. This outcome is consistent with the previous studies as clathrin-mediated endocytosis [36]. In fact, a characteristic feature of the mannose receptor is its rapid internalization from the plasma membrane via a clathrin-mediated mechanism that delivers the receptors to the endocytic pathway [37]. Moreover, mannose receptor may contribute to the internalization of mannosylated particles and pathogens [38]. Similar to chlatrin-mediated endocytosis, the mannosylated ligands bind to the mannose receptor at the cell surface and then are internalized into the cell, where it dissociates from the receptor in an acidic endosomal compartment.

The *in vitro* cell uptake and pathway mechanism studies revealed that mannosylation improved the SLNs uptake overtime and that process was energy-dependent, mainly by clathrin-mediated endocytosis. This aspect is relevant to understand the fate of SLNs and M-SLNs during the endocytic process, as clathrin endocytosis mechanism mediates the NPs

trafficking to endosomes, followed by degradation processes in late endosomes and lysosomes.

Conclusion

In this study, a new delivery strategy for the treatment of TB based in mannosylated SLNs containing the front-line anti-TB drug RIF was developed. The SLNs formulations were developed to improve the drug uptake by the macrophages and can be administered by inhalation, aiming to improve the patient compliance and consequently, the success of this long-duration therapy. The developed mannosylated SLNs possess a diameter of approximately 250 nm, which is considered to be suitable for the lung deposition and macrophage phagocytosis. Moreover, SLNs present a high zeta potential of around |30| mV, indicating a good stability. The functionalization of SLNs with mannose was confirmed by the zeta potential variations between the uncoated and the mannosylated SLNs and also by the FTIR spectrum analysis that allowed the detection of the Schiff's base. The RIF EE was high, being 70% for SLNs and 90% for M-SLNs. TEM analysis demonstrated that all SLNs presented a spherical morphology. DSC studies revealed that the incorporation of the drug and mannose induced a disturbance in the crystal order of the lipid matrix of the SLNs. A sustained release profile of SLNs in simulated pulmonary fluids was achieved, with more than 80% of RIF remained entrapped inside the SLNs lipid matrix after 8 h. In addition, stability studies revealed slight variations in terms of the physicochemical properties of SLNs

over a period of six months, reinforcing the stability of the lipid NPs.

The cytotoxicity results showed that neither SLNs-RIF nor M-SLNs-RIF, and their unloaded formulations were considered toxic for THP1 macrophages, and could be used to safely delivery RIF. Besides, the high degree of internalization in human macrophages, especially for M-SLNs-RIF, suggested an effective targeting of mannose receptors of the developed system.

In conclusion, the overall results suggest that mannosylated SLNs constitute suitable carriers for the inhalatory administration of RIF, protecting it from the pulmonary fluids and increasing drug's bioavailability. Thus, the developed SLNs constitute an affordable technology that holds great promise for a future clinical application in the TB treatment.

Acknowledgements

Disclosure statement

No potential conflict of interest was reported by the authors.

Funding

ORCID

Alexandre C. C. Vieira (iD) http://orcid.org/0000-0002-9399-8169
Luíse L. Chaves (iD) http://orcid.org/0000-0002-1197-7306
Marina Pinheiro (iD) http://orcid.org/0000-0002-6931-1355
Sofia A. Costa Lima (iD) http://orcid.org/0000-0001-8777-5877
Domingos Ferreira (iD) http://orcid.org/0000-0001-6200-7169
Bruno Sarmento (iD) http://orcid.org/0000-0001-5763-7553
Salette Reis (iD) http://orcid.org/0000-0002-0736-2835

References

[1] Kaur MS, Garg T, Narang R. A review of emerging in the treatment of tuberculosis. Artif Cell Nanomed B. 2014;44:478–484.

[2] WHO. Global tuberculosis report 2016. Switzerland: WHO Library Cataloguing-in-Publication Data; 2016.

[3] Cadena AM, Flynn JL, Fortune SM. The importance of first impressions: early events in Mycobacterium tuberculosis infection influence outcome. mBio. 2016;7:1–9.

[4] Flynn JL, Chan J, Lin PL. Macrophages and control of granulomatous inflammation in tuberculosis. Mucosal Immunol. 2011;4:271–278.

[5] Costa A, Pinheiro M, Magalhães J, et al. The formulation of nanomedicines for treating tuberculosis. Adv Drug Deliv Rev. 2016;102:102–115.

[6] Kolyva AS, Karakousis PC. Old and new TB drugs: mechanisms of action and resistance, understanding tuberculosis – new approaches to fighting against drug resistance. London, UK: InTech; 2012.

[7] Zumla A, Chakaya J, Centis R, et al. Tuberculosis treatment and management – an update on treatment regimens, trials, new drugs, and adjunct therapies. Lancet Respir Med. 2015;3:220–234.

[8] Zumla A, Nahid P, Cole ST. Advances in the development of new tuberculosis drugs and treatment regimens. Nat Rev Drug Discov. 2013;12:388–404.

[9] Arun B, Narendar D, Veerabrahma K. Development of olmesartan medoxomil lipid-based nanoparticles and nansuspension: preparation, characterization and comparative pharmacokinetic evaluation. Artif Cell Nanomed B. 2017;46:126–137.

[10] Radtke M, Souto EB, Muller RH. Nanostructured lipid carriers – a novel generation of solid lipid drug carriers. Pharm Technol Eur. 2015;17:45–50.

[11] Pinheiro M, Ribeiro R, Vieira A, et al. Design of a nanostructured lipid carrier intended to improve the treatment of tuberculosis. Drug Des Devel Ther. 2016;10:2467–2475.

[12] Irache JM, Salman HH, Gamazo C, et al. Mannose-targeted systems for the delivery of therapeutics. Expert Opin Drug Deliv. 2008;5:703–724.

[13] Ferreira M, Silva E, Barreiros L, et al. Methotrexate loaded lipid nanoparticles for topical management of skin-related diseases: design, characterization and skin permeation potential. Int J Pharm. 2016;512:14–21.

[14] Jain A, Agarwal A, Majumder S, et al. Mannosylated solid lipid nanoparticles as vectors for site-specific delivery of an anti-cancer drug. J Control Release. 2010;148:359–367.

[15] Vieira AC, Chaves LL, Pinheiro M, et al. Design and statistical modeling of mannose-decorated dapsone-containing nanoparticles as a strategy of targeting intestinal M-cells. Int J Nanomedicine. 2016;11:2601–2617.

[16] Varshosaz J, Eskandari S, Tabbakhian M. Freeze-drying of nanostructure lipid carriers by different carbohydrate polymers used as cryoprotectants. Carbohydr Polym. 2012;88:1157–1163.

[17] Olena I, Emerson C, Barbara P, et al. Influence of silver content on rifampicin adsorptivity for magnetite/Ag/rifampicin nanoparticles. Nanotechnology. 2017;28:055603.

[18] Pinheiro M, Pisco S, Silva AS, et al. Evaluation of the effect of rifampicin on the biophysical properties of the membranes: significance for therapeutic and side effects. Int J Pharm. 2014;166:190–197.

[19] Shah RM, Bryant G, Taylor M, et al. Structure of solid lipid nanoparticles produced by a microwave-assisted microemulsion technique. RSC Adv. 2016;6:36803–36810.

[20] Singh SK, Dadhania P, Vuddanda PR, et al. Intranasal delivery of asenapine loaded nanostructured lipid carriers: formulation, characterization, pharmacokinetic and behavioural assessment. RSC Adv. 2016;6:2032–2045.

[21] Barros D, Costa Lima SA, Cordeiro-da-Silva A. Surface functionalization of polymeric nanospheres modulates macrophage activation: relevance in leishmaniasis therapy. Nanomedicine (Lond). 2015;3:387–403.

[22] Cho M, Cho WS, Choi M, et al. The impact of size on tissue distribution and elimination by single intravenous injection of silica nanoparticles. Toxicol Lett. 2009;189:177–183.

[23] Chow AH, Tong HH, Chattopadhyay P, et al. Particle engineering for pulmonary drug delivery. Pharm Res. 2007;24:411–437.

[24] Neves AR, Lúcio M, Martins S, et al. Novel resveratrol nanodelivery systems based on lipid nanoparticles to enhance its oral bioavailability. Int J Nanomedicine. 2013;8:177–187.

[25] Müller H, Jacobs C, Kayser O. Nanosuspensions as particulate drug formulations in therapy: rationale for development and what we can expect for the future. Adv Drug Deliv Rev. 2001;23:3–19.

[26] Silva AC, Kumar A, Wild W, et al. Long-term stability, biocompatibility and oral delivery potential of risperidone-loaded solid lipid nanoparticles. Int J Pharm. 2012;436:798–805.

[27] Vivek K, Reddy H, Murthy RSR. Investigations of the effect of the lipid matrix on drug entrapment, in vitro release, and physical stability of olanzapine-loaded solid lipid nanoparticles. AAPS PharmSciTech. 2007;8:16–24.

[28] Andreani T, Kiill CP, de Souza ALR, et al. Surface engineering of silica nanoparticles for oral insulin delivery: characterization and cell toxicity studies. Colloids Surf B Biointerfaces. 2014;123: 916–923.

[29] Yamori S, Ichiyama S, Shimokata K, et al. Bacteriostatic and bactericidal activity of antituberculosis drugs against Mycobacterium tuberculosis, Mycobacterium avium-Mycobacterium intracellulare complex and Mycobacterium kansasii in different growth phases. Microbiol Immunol. 1992;36:361–368.

[30] Chai GH, Hu FQ, Sun J, et al. Transport pathways of solid lipid nanoparticles across Madin − Darby canine kidney epithelial cell monolayer. Mol Pharm. 2014;11:3716–3726.

[31] Beloqui A, Solinís MÁ, Gascón AR, et al. Mechanism of transport of saquinavir-loaded nanostructured lipid carriers across the intestinal barrier. J Control Release. 2013;166:115–123.

[32] Lopes-de-Araújo J, Neves AR, Gouveia VM, et al. Oxaprozin-loaded lipid nanoparticles towards overcoming NSAIDs side-effects. Pharm Res. 2016;33:301–134.

[33] Neves AR, Queiroz JF, Costa Lima SA, et al. Cellular uptake and transcytosis of lipid-based nanoparticles across the intestinal barrier: relevance for oral drug delivery. J Colloid Interface Sci. 2016;463:258–265.

[34] Moretton MA, Chiappetta DA, Andrade F, et al. Hydrolyzed galactomannan-modified nanoparticles and flower-like polymeric micelles for the active targeting of rifampicin to macrophages. J Biomed Nanotechnol. 2013;9:1076–1087.

[35] Sahay G, Alakhova DY, Kabanov AV. Endocytosis of nanomedicines. J Control Release. 2010;145:182–195.

[36] Ruge CA, Hillaireau H, Grabowski N, et al. Pulmonary surfactant protein A-mediated enrichment of surface-decorated polymeric nanoparticles in alveolar macrophages. Mol Pharmaceutics. 2016;13:4168–4178.

[37] Zvaritch E, Lambeau G, Lazdunski M. Endocytic properties of the M-type 180-kDa receptor for secretory phospholipases A2. J Biol Chem. 1996;271:250–225.

[38] Linehan SA, Martinez-Pomares L, da Silva RP, et al. Endogenous ligands of carbohydrate recognition domains of the mannose receptor in murine macrophages, endothelial cells and secretory cells; potential relevance to inflammation and immunity. Eur J Immunol. 2001;31:1857–1866.